Ultra-narrow photonic nanojets through a glass cuboid embedded in a dielectric cylinder

JIANMING YANG,[1,2,*] PATRICE TWARDOWSKI,[1] PHILIPPE GÉRARD,[1] YI DUO,[3] JOËL FONTAINE,[1] AND SYLVAIN LECLER[1]

[1]ICube UMR-7357, CNRS, University of Strasbourg, INSA Strasbourg-Illkirch, France
[2]Changchun Institute of Optics, Fine Mechanics and Physics, Chinese Academy of Sciences, Changchun, Jilin 130033, China
[3]Institute of Ocean Research, Peking University, Beijing, 100871, China
*jianming.yang@unistra.fr

Abstract: A glass cuboid, embedded inside a dielectric cylinder is studied when illuminated with a monochromatic plane wave. A photonic nanojet (PNJ) with a full-width at half-maximum (FWHM) waist of around $0.25\lambda_0$ is obtained outside the external surface of the cuboid. The influence of the parameters of a square section cuboid is studied. Three particular phenomena can be obtained and are discussed: an ultra-narrow PNJ on the external surface of the cuboid, a long photonic jet and the excitation of whispering gallery modes (WGMs). A parametric study, over the width and the height of a rectangular section cuboid, shows that these parameters can be used to control the photonic jet properties. We also study several other geometries of the insert, which shows that the key parameter is the refractive index of the inserted material. Finally, we show that by changing the incident angle we can obtain a curved photonic jet.

References and links

1. Z. Chen, A. Taflove, and V. Backman, "Photonic nanojet enhancement of backscattering of light by nanoparticles: a potential novel visible-light ultramicroscopy technique," Opt. Express **12**(7), 1214–1220 (2004).
2. G. Mie, "Beiträge zur Optik trüber Medien, speziell kolloidaler Metallösungen," Ann. Phys. **330**(3), 377–445 (1908).
3. X. Li, Z. Chen, A. Taflove, and V. Backman, "Optical analysis of nanoparticles via enhanced backscattering facilitated by 3-D photonic nanojets," Opt. Express **13**(2), 526–533 (2005).
4. S. Lecler, Y. Takakura, and P. Meyrueis, "Properties of a three-dimensional photonic jet," Opt. Lett. **30**(19), 2641–2643 (2005).
5. S. Yang, A. Taflove, and V. Backman, "Experimental confirmation at visible light wavelengths of the backscattering enhancement phenomenon of the photonic nanojet," Opt. Express **19**(8), 7084–7093 (2011).
6. S. Lecler, S. Haacke, N. Lecong, O. Crégut, J.-L. Rehspringer, and C. Hirlimann, "Photonic jet driven non-linear optics: example of two-photon fluorescence enhancement by dielectric microspheres," Opt. Express **15**(8), 4935–4942 (2007).
7. P. Ferrand, J. Wenger, A. Devilez, M. Pianta, B. Stout, N. Bonod, E. Popov, and H. Rigneault, "Direct imaging of photonic nanojets," Opt. Express **16**(10), 6930–6940 (2008).
8. D. Grojo, N. Sandeau, L. Boarino, C. Constantinescu, N. De Leo, M. Laus, and K. Sparnacci, "Bessel-like photonic nanojets from core-shell sub-wavelength spheres," Opt. Lett. **39**(13), 3989–3992 (2014).
9. S. Lee, L. Li, and Z. Wang, "Optical resonances in microsphere photonic nanojets," J. Opt. **16**(1), 015704 (2014).
10. Y. E. Geints, E. Panina, and A. Zemlyanov, "Control over parameters of photonic nanojets of dielectric microspheres," Opt. Commun. **283**(23), 4775–4781 (2010).
11. H. Guo, Y. Han, X. Weng, Y. Zhao, G. Sui, Y. Wang, and S. Zhuang, "Near-field focusing of the dielectric microsphere with wavelength scale radius," Opt. Express **21**(2), 2434–2443 (2013).
12. A. Devilez, B. Stout, N. Bonod, and E. Popov, "Spectral analysis of three-dimensional photonic jets," Opt. Express **16**(18), 14200–14212 (2008).

13. A. Heifetz, J. J. Simpson, S.-C. Kong, A. Taflove, and V. Backman, "Subdiffraction optical resolution of a gold nanosphere located within the nanojet of a Mie-resonant dielectric microsphere," Opt. Express **15**(25), 17334–17342 (2007).
14. A. V. Itagi and W. A. Challener, "Optics of photonic nanojets," J. Opt. Soc. Am. A **22**(12), 2847–2858 (2005).
15. V. Pacheco-Peña, M. Beruete, I. V. Minin, and O. V. Minin, "Multifrequency focusing and wide angular scanning of terajets," Opt. Lett. **40**(2), 245–248 (2015).
16. M. X. Wu, B. J. Huang, R. Chen, Y. Yang, J. F. Wu, R. Ji, X. D. Chen, and M. H. Hong, "Modulation of photonic nanojets generated by microspheres decorated with concentric rings," Opt. Express **23**(15), 20096–20103 (2015).
17. B. Yan, L. Yue, and Z. Wang, "Engineering near-field focusing of a microsphere lens with pupil masks," Opt. Commun. **370**, 140–144 (2016).
18. M. Wu, R. Chen, J. Soh, Y. Shen, L. Jiao, J. Wu, X. Chen, R. Ji, and M. Hong, "Super-focusing of center-covered engineered microsphere," Sci. Rep. **6**(1), 31637 (2016).
19. L. Yue, B. Yan, J. N. Monks, Z. Wang, N. T. Tung, V. D. Lam, O. Minin, and I. Minin, "Production of photonic nanojets by using pupil-masked 3D dielectric cuboid," J. Phys. D Appl. Phys. **50**(17), 175102 (2017).
20. L. Yue, B. Yan, and Z. Wang, "Photonic nanojet of cylindrical metalens assembled by hexagonally arranged nanofibers for breaking the diffraction limit," Opt. Lett. **41**(7), 1336–1339 (2016).
21. G. Gu, J. Song, H. Liang, M. Zhao, Y. Chen, and J. Qu, "Overstepping the upper refractive index limit to form ultra-narrow photonic nanojets," Sci. Rep. **7**(1), 5635 (2017).
22. B. S. Luk'yanchuk, R. Paniagua-Domínguez, I. Minin, O. Minin, and Z. Wang, "Refractive index less than two: photonic nanojets yesterday, today and tomorrow," Opt. Mater. Express **7**(6), 1820–1847 (2017).
23. V. Pacheco-Peña, M. Beruete, I. V. Minin, and O. V. Minin, "Terajets produced by dielectric cuboids," Appl. Phys. Lett. **105**(8), 084102 (2014).
24. I. Minin, O. Minin, I. Nefedov, V. Pacheco-Peña, and M. Beruete, "Beam compressed system concept based on dielectric cluster of self-similar three-dimensional dielectric cuboids," in *2016 Global Symposium on Millimeter Waves (GSMM) & ESA Workshop on Millimetre-Wave Technology and Applications* (IEEE, 2016), pp. 1–2.
25. H. H. Nguyen Pham, S. Hisatake, O. V. Minin, T. Nagatsuma, and I. V. Minin, "Enhancement of spatial resolution of terahertz imaging systems based on terajet generation by dielectric cube," APL Photonics **2**(5), 056106 (2017).
26. I. Mahariq and H. Kurt, "Strong field enhancement of resonance modes in dielectric microcylinders," J. Opt. Soc. Am. B **33**(4), 656–662 (2016).
27. I. V. Minin and O. V. Minin, *Diffractive Optics and Nanophotonics* (Springer International Publishing, 2016).

1. Introduction

The photonic nanojet (PNJ) was first reported by Chen et al. in 2004 through finite-difference time-domain (FDTD) modeling of cylindrical structures under plane wave illumination [1]. They found that a full width at half maximum (FWHM) that was slightly smaller than $\lambda_0/2$ can be generated by a transparent dielectric microcylinder with a wavelength-scale radius, where λ_0 is the wavelength in free space. The exact solution of Maxwell's equations for a dielectric microsphere was obtained by Gustav Mie in 1908 [2]. Applying this method, PNJ in the 3D case of a dielectric sphere was first reported by Li et al. [3]. Lecler et al. applied Mie theory to analyze the general three-dimensional properties of photonic nanojets generated by plane-wave illuminated dielectric microspheres in free space [4]. The key parameters of PNJs which are their FWHM, focal distance, decay length, and light intensity, have been the subject of extensive theoretical and experimental studies [5–14]. These studies indicate that the electric field distribution of the PNJ depends on the radius and refractive index of the microspheres or cylinders, and the incident wavelength in the surrounding medium. More recently, the possibility of obtaining PNJ using cuboid particles has also been demonstrated [15].

To improve the optical properties and in particular to reduce the FWHM of PNJs, several designs have been proposed. Wu et al. used microspheres decorated with concentric rings to modulate PNJs [16]. The average ring width (outer ring radius minus inner ring radius) was about 0.25 μm. They obtained experimentally a $0.485\lambda_0$ FWHM. Yan et al. applied a pupil mask to cover the center of the microsphere. The FWHM can be reduced to about $0.3\lambda_0$ but the maximum intensity was also reduced [17]. This concept was later proven experimentally by Wu et al. [18] with a FWHM of $0.387\lambda_0$. A similar concept was also applied to a 3D dielectric cuboid demonstrating a reduced FWHM ($0.374\lambda_0$ with 75% mask) [19]. Yue et al. reported a reduction of the FWHM ($0.244\lambda_0$) using cylindrical metalenses assembled by

hexagonally arranged nanofibers [20]. Recently, ultra-narrow PNJs (0.287 λ_0) generated by overstepping the upper refractive index limit have been proposed by Gu et al. [21]. A review of PNJs has been made by B. S. Luk'yanchuk [22].

Apart from micro particles with high degree of symmetry as spheres and cylinders, cuboids can also produce such PNJs [23]. Moreover, the cube can form a different PNJ with subwavelength size when it is located in the focus of another similar cube [24, 25]. PNJ with FWHM of 0.55λ_0 was demonstrated. I. Mahariq et al. have studied field enhancement of resonance modes in dielectric microcylinders and have simulated a dielectric cuboid inserted in the center of microcylinders [26]. They have shown whispering gallery modes (WGMs) can be generated in certain cases while the PNJ behavior seems to disappear.

In this paper, the embedded transparent dielectric cuboid is placed near the boundary of the transparent dielectric cylinder. A FWHM of around half the Abbe diffraction limit can be obtained. Comparing to the geometry proposed in Ref [24, 25], the cuboid can be considered as locates also near a focal position. However, in our proposed design, the cuboid is immersed not in air, but in the medium of a cylinder, which produce different results. By modifying the size and refractive index of the square section cuboid, we observe: an ultra-narrow PNJ on the external surface of the cuboid, a long photonic jet and the excitation of WGMs. Then considering a rectangular section of the cuboid, we show that the width and the height of the cuboid can be used to adjust the PNJ properties. We also study several other geometries of the insert, which shows that the key parameter is the refractive index of the inserted material. Finally, with a square section cuboid we show that by changing the incident angle a curved photonic jet (hook effect) can be obtained.

2. Ultra-narrow Photonic nanojet

An infinite long transparent dielectric square section cuboid embedded in a transparent dielectric cylinder is illuminated by a monochromatic linear polarized plane wave with an incident wave vector k parallel to the x axis. Its polarization direction is parallel to the axis of the cylinder, the z axis. The cylinder is tangential to the center of the outer surface of the cuboid. The electric field distribution is obtained numerically by a finite element method (FEM) with COMSOL Multiphysics. We use free triangular mesh with a maximum mesh size of $\lambda_0/(15n)$, where n is the refractive index of the corresponding medium. We apply perfect matched layers (PMLs) as the boundary conditions in the four sides. The incident field is introduced as background, and the scattered field is computed. All the results below concern the total field. Figure 1 shows the simulated PNJ when the radius of the cylinder r is 2.5 μm, the square section side of the cuboid a is 1 μm and the refractive indices of the cylinder n_1 and the cuboid n_2 are 1.5 and 1.8 respectively. The illumination wavelength λ_0 is 0.5 μm. The results of the simulation give a FWHM equal to 150 nm. The electric field intensity is shown in Fig. 1(a) assuming a unitary incident intensity. Streamlines of Poynting vectors are shown in Fig. 1(b). The insert is the zoomed image around the focal position confirming that the phenomenon is related to propagating waves. The color scale represents the Px values.

The corresponding electric field intensity profile (the blue curve) on the focal plane is shown in Fig. 1(c) and its distribution along the x-axis is shown in Fig. 1(d). As a reference, we also plot the case of a single full cylinder with an index of n = 1.5 (the green curve). L is the working distance from the external surface of the cuboid to the position of maximum intensity. D is the decay length from the point of the maximum light intensity I_{max} to 1/e value of I_{max}. Compared with the reference curve, the FWHM is reduced by 36% from 235 nm (0.47λ_0) to 150 nm (0.3λ_0), the maximum intensity is increased by about 17% and L is reduced from 455 nm to 32 nm. D is reduced from 2.2λ_0 to 0.7λ_0. We notice that both L and D diminish with the reduction of FWHM, as in Ref [16–21]. This phenomenon can be compared to the result obtained with a conventional lens for which higher numerical aperture corresponds to a shorter focal length for a constant lens diameter.
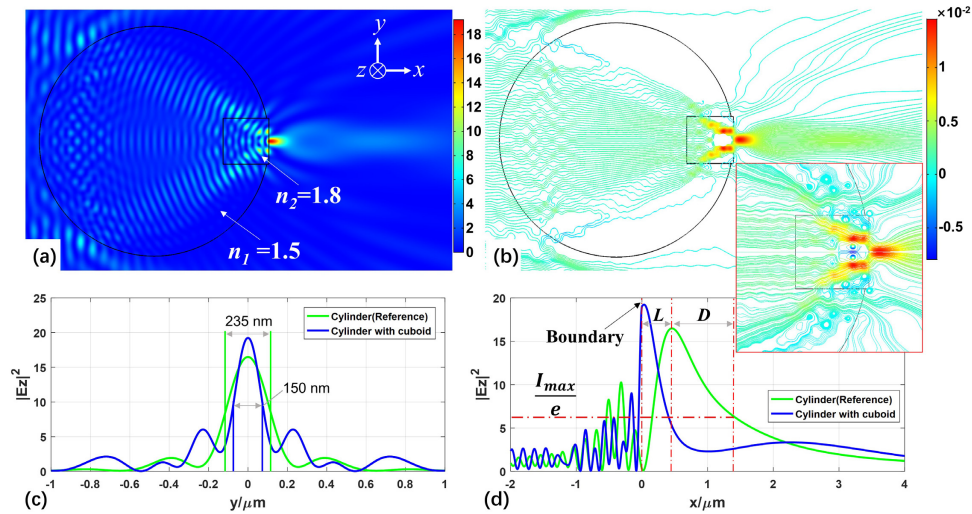
Fig. 1. Dielectric cuboid embedded in a dielectric cylinder. The wavelength of the illumination plane wave is 0.5 μm. The radius of the cylinder is r = 2.5 μm. The cuboid has a square section of side a = 1 μm. The refractive indices of the cylinder and the cuboid are n_1 = 1.5 and n_2 = 1.8 respectively. (a) The electric field intensity $|E|^2$. (b) Streamlines of the Poynting vectors. The insert is the zoomed image around the focal position. The color scale represents the value of the P_x component. (c) Electric field intensity $|E|^2$ on the focus width. In green: reference for a single full cylinder with an index of n = 1.5. In blue: new design shown in (a). (d) The electric field intensity distribution $|E|^2$ along x. L represents the distance between the position of the maximum intensity and the external surface of the cuboid. L = 455 nm for the reference case and L = 32 nm for the new design. D is the decay length from the point of the maximum light intensity I_{max} to 1/e value of I_{max}.

3. Parametric study of the cuboid

We first consider a square section cuboid with a side increasing from a = 0.1 μm to 1.5 μm with a step size Δa = 0.02 μm. Its refractive index is changed from n_2 = 1.4 to n_2 = 1.9 with steps of Δn = 0.1. The FWHM ratio ($FWHM / \lambda_0$) is calculated around the maximum intensity position outside of the cuboid. The results in Fig. 2 show the FWHM, the distance of the maximum intensity position L and the maximum electric field intensity $|E|^2$ outside of the cuboid as a function of the cylinder size parameter, the cuboid size and refractive. The refractive index of the cylinder is n_1 = 1.5 in all cases. The cylinder size parameter is defined as $q = 2\pi r / \lambda_0$. The curve when $n_2 = n_1$ = 1.5 (green curve) serves as a reference.

From Fig. 2, a certain amount of useful information can be deduced. Firstly, the FWHM decreases with an increase in the refractive index of the cuboid. Then, the FWHM is smaller than the cylinder alone mostly when the cuboid has a higher refractive index than the cylinder. For example, the case already discussed in Fig. 1 is indicated by a star with number 0. The smallest FWHMs occur when $n_2 \geq 1.8$, and the maximum intensity can reach the external surface of the cuboid. As we have only represented the intensity outside of the cuboid, the position of the maximum intensity may be inside. The smallest FWHM ratio is around $0.25\lambda_0$ with n_2 = 1.9 and with a rather large cuboid ($a > 2\lambda_0$ for q = 39.3). One example is indicated with the red star number 1 in Fig. 2(a). Its electric field intensity distribution and Poynting vector streamlines are represented in Fig. 3 as for two other cases. We can notice in Fig. 3(a) that the light in the PNJ is still a propagating wave despite it being an ultra-narrow PNJ. Two local maxima can be observed along the optical axis, showing that constructive interference contributes to this ultra-narrow PNJ.
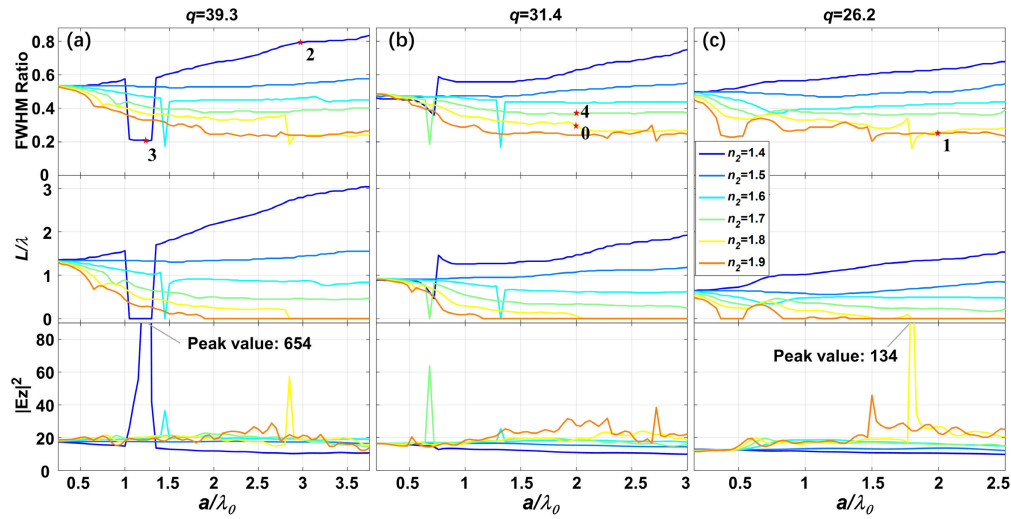
Fig. 2. FWHM ratio (FWHM/λ_0) of the maximum intensity spot, maximum intensity position L and maximum electric field intensity $|E|^2$ out of the cuboid vs the cylinder size parameter q and the side a of the cuboid in λ unit. Different colors represent different refractive indices n_2 of the cuboid, which is indicated in the center of the figure. The refractive index of the cylinder is 1.5 in all cases. The red stars are representative points that are studied separately. (a) cylinder size parameter $q = 39.3$; (b) $q = 31.4$ and (c) $q = 26.2$.

On the other hand, when $n_2 < n_1$, Fig. 2 shows that the FWHM ratio of the PNJ is usually larger than for the cylinder alone. L is also larger, and the maximum intensity is lower. In Fig. 3(b) an example is given corresponding to star point 2. This corresponds to a longer photonic jet: the decay length of the jet is 300% longer, the intensity of the jet is 36% lower and the FWHM is 145% larger than the full cylinder alone. Therefore, we can control the FWHM ratio and L flexibly by choosing required values of n_2 and a.

Finally, some very specific cases give very high peak intensities and a narrow FWHM. For example, the star point 3 is represented Fig. 3(c). This corresponds to a WGM inside the cylinder with very high intensity values compared to the previously studied PNJs. By definition, a WGMs is evanescent in the radial direction and stationary in the angular one. This is the reason why the WGM is visible on the $|E|^2$ map (Fig. 3(c) left) but not in the Poynting vector map (Px component of the Poynting vector in Fig. 3(c) right). We see that despite the WGM resonance, a PNJ is still happened outside. Its intensity is weak comparing to the WGM so that we cannot observe it in the figure of electric field intensity, but we can observe it from the Poynting vectors streamlines. There is an interval for size a when $n_2 = 1.4$, where the FWHM ratio is around 0.2 and the distance L is 0. These cases also correspond to WGMs, which indicates that WGMs can be generated more easily in this kind of configuration. For the three particular cases depicted in Fig. 3, the magnitude of the Px component of the Poynting vector is almost the same as when the WGMs create a high electric field intensity.
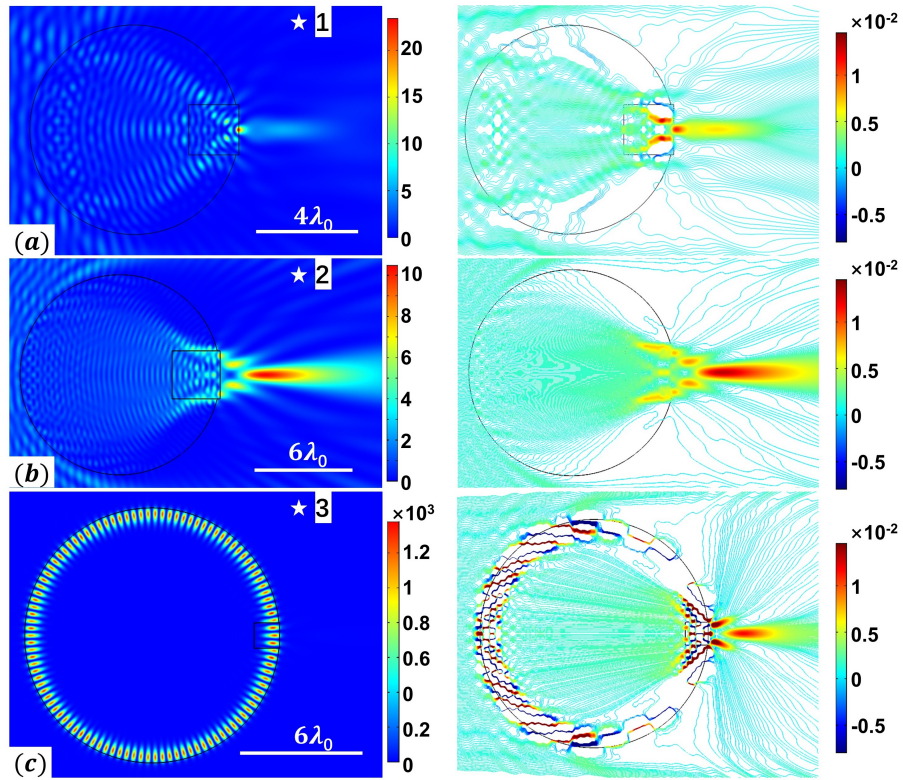
Fig. 3. Electric field intensity $|Ez|^2$ and Poynting vectors streamlines for several specific cases (marked with stars) referenced in Fig. 2. (a) $n_2 = 1.9$, $a = 2\lambda_0$ and $q = 26.2$. (b) $n_2 = 1.4$, $a = 3\lambda_0$ and $q = 39.3$ (c) $n_2 = 1.4$, $a = 1.25\lambda_0$ and $q = 39.3$.
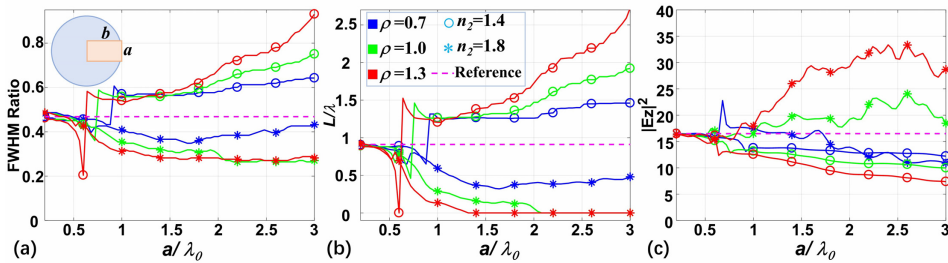

Fig. 4. Characteristics of the focal spot vs the cuboid geometry. (a) FWHM ratio of the maximum intensity spot, (b) maximum intensity position L and (c) maximum electric field intensity $|Ez|^2$ out of the cuboid vs the height a. Different colors represent different values of ρ and different marks represent different refractive indices n_2 of the cuboid, which is indicated in the center of the figure. The refractive index of the cylinder is 1.5 in all cases. The illumination wavelength is $\lambda_0 = 0.5\,\mu m$. The reference corresponds to a cylinder of refractive index $n_1 = 1.5$.

We now consider rectangular section cuboids with height a and width b defined along their y and x axes respectively as shown in the insert of Fig. 4(a). We define the parameter ρ equal to b/a. In Fig. 4, the FWHM Ratio, the distance of the maximum intensity position L and the maximum electric field intensity $|E|^2$ outside of the cuboid ($L>0$) are shown as a function of a, n_2 and ρ. If $n_2>n_1$, we notice that for a constant height a, as ρ increases, the focal spot becomes smaller and closer to the external surface of the cuboid with a higher intensity, while the focal spot becomes larger and further with a lower intensity if $n_2< n_1$. More generally, the width and the height of a rectangular section cuboid are additional

parameters that can be used to control the PNJ properties (FWHM ratio, peak intensity and distance L from the cuboid).

4. Alternative geometries of the dielectric insert

We have also investigated some alternative geometries that can also reduce the FWHM as shown in Fig. 5. The reference case related to star number 4 in Fig. 2 is shown in Fig. 5(a) where the size of the cuboid is $2\lambda_0$. In Fig. 5(b) the insert is similar to a cuboid with a side length of $a = 2\lambda_0$, but with an external surface fitting the host cylinder shape. In Fig. 5(c) the left surface of the original cuboid ($a = 2\lambda_0$) is replaced by a cylinder with a radius equals to λ_0 and the right surface has a surface fitting the host cylinder shape. Finally, we have investigated the case where the inclusion is a cylinder with $1.4\lambda_0$ radius tangent to the larger cylinder. For all cases, the refractive index of the inserts is 1.7. The FWHM ratio and maximum intensity position L are given in the upper right corner of each figure.
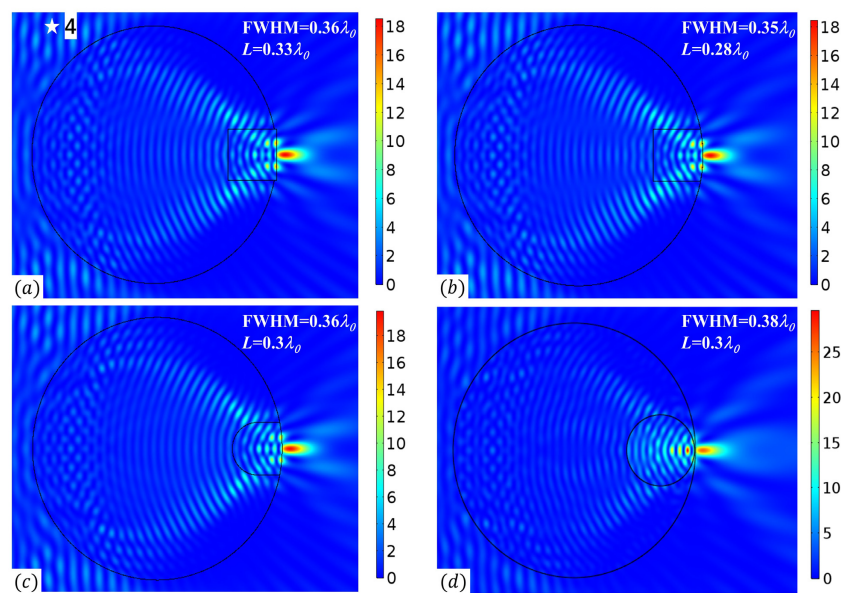

Fig. 5. Alternative geometries that can reduce the FWHM. The refractive index of all the inserts is 1.7. The FWHM ratio and maximum intensity position L are given in the upper right corner of each figure. (a) Case corresponding to star number 4 in Fig. 2. The side length $a = 2\lambda_0$. (b) The insert is similar to a cuboid with a side length of $a = 2\lambda_0$, but with an external surface fitting the host cylinder shape. (c) The left surface of the original cuboid ($a = 2\lambda_0$) is replaced by a cylinder with a radius equals to λ_0 and the right surface is a surface fitting the host cylinder shape. (d) The inclusion is a cylinder with $1.4\lambda_0$ radius tangent to the larger cylinder.

We notice that the FWHM in all cases are similar and smaller than the Abbe diffraction limit. This indicates that the dominant reason for the reduction of FWHM is the larger refractive index of the insert rather than its shape. For a single cylinder, we know that the FWHM decreases with increasing of its refractive index. However, too high index will focus inside the cylinder, which limits the further reduction of the FWHM. In the proposed system, by putting the higher index insert near the focus, we benefit the reduction of the FWHM from high index and avoid a focus point inside the system. Meanwhile, as the reduction of FWHM is not sensitive to the shape of the insert, the tolerance of fabrication is better. To fabricate such a system, plasma-ion implantation or the use of an ion implantation Van der Graaf, both with mask could be used.

5. Incident angle and photonic hook

When the direction of the illumination light is different from Fig. 1(along the *x* axis), but with the same geometry and parameters, the electric field intensity distribution also changes as shown in Fig. 6. Equivalently, for the sake of simplicity, the direction of the illumination light remains unchanged and the cuboid is rotated with an angle θ. Figure 6 represents the electric field intensity distributions and streamlines of Poynting vectors for three different angles (a) $\theta = 11°$, (b) $\theta = 70°$, (c) $\theta = 180°$. For the case where θ is less than 11° the maximum electric field intensity and the FWHM of the jet are almost similar compared to the normal incident case as shown in Fig. 1. For $\theta = 11°$, there are two or three separate focal points in Fig. 6(a). The most intense jet is due to the cuboid and is distorted. The position of the maximum intensity rotates as the cuboid rotates. The second focus is weaker and due to the cylinder. When θ is around 70°, the shape of the photonic jet is curved as shown in Fig. 6(b). This effect has been referred to as a photonic hook [27]. This can be understood as an interference phenomenon, which takes place in the caustic and is caused by the break of the symmetry. Another interpretation corresponds to an analogy with off-axis aberration, mainly coma. When the cuboid moves to the opposite side ($\theta = 180°$), a photonic jet created by the cuboid inside the cylinder and three jets outside the cylinder can be observed, as shown in Fig. 6(c). This last phenomenon was observed in Ref [26]. If the high intensity of the focal spot and the small FWHM are the required parameters, the maximum illumination angle should be less than 11°. If a curved photonic jet, like a photonic hook, is sought for, the shape of the jet can be modified by choosing the angle θ to be around 70°. Here we give particular angle values for the example of Fig. 1. Nevertheless, they also depend on the refractive indices and the section sizes of the cuboid.
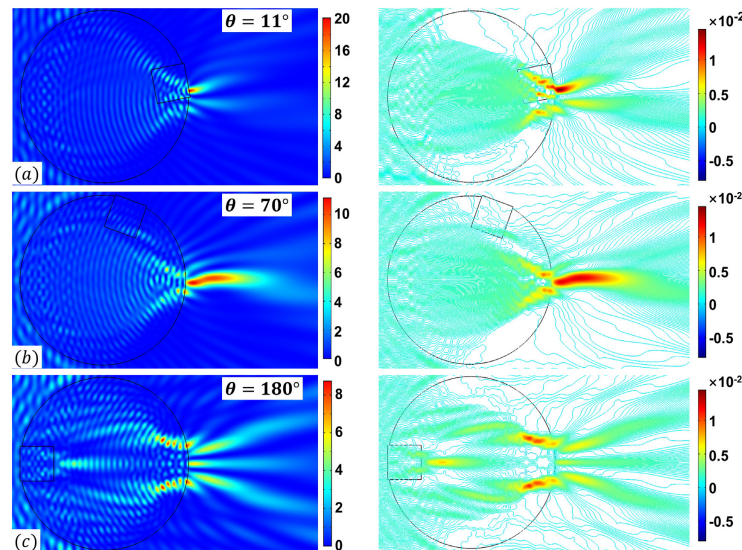

Fig. 6. Effect of the incidence angle. The illumination light flows from left to right. θ is the cuboid rotation angle compared to Fig. 1. As in Fig. 1, the wavelength of the illumination plane wave is 0.5 μm. The radius of the cylinder is r = 2.5 μm. The cuboid has a square section of side a = 1 μm. The refractive indices of the cylinder and the cuboid are n_1 = 1.5 and n_2 = 1.8 respectively. (Left) Electric field intensity $|E|^2$ and (right) streamline of Poynting vectors for several rotation angles. (a) $\theta = 11°$, (b) $\theta = 70°$, (c) $\theta = 180°$.

6. Conclusion

In summary, we have presented a design that can achieve a PNJ with a FWHM of around half that of the Abbe diffraction limit. In this geometry a dielectric cuboid is embedded inside a

dielectric cylinder. In this configuration a PNJ is created and focused outside the cuboid. A parameter study of the side and refractive index of a square section cuboid has been presented, demonstrating that smaller PNJs can be obtained with higher cuboid refractive indices. Three particular cases have been selected and discussed: an ultra-narrow PNJ on the external surface of the cuboid, a long photonic jet and the excitation of WGMs. Considering a rectangular section cuboid, if the refractive index of the cuboid is greater than the cylinder index, it can be noticed that for a constant height, as the ratio width over height increases, the focal spot becomes smaller and closer to the external surface of the cuboid and with a higher intensity. We have also investigated several alternative geometries of the insert, which demonstrate that the shape of the insert is not so critical for the reduction of FWHM. To fabricate such a system, ion implantation with mask could be used. Finally, we have shown that by changing the incident angle, a curved photonic jet can be obtained, an effect known as a photonic hook. This may be used to manipulate nano-objects.